universe

IMPACT FACTOR 2.813

CITESCORE 3.2

Article

Weak Deflection Angle by Kalb–Ramond Traversable Wormhole in Plasma and Dark Matter Mediums

Wajiha Javed, Hafsa Irshad, Reggie C. Pantig and Ali Övgün

Special Issue

Elementary Particles in Astrophysics and Cosmology

Edited by

Prof. Dr. Daniele Fargion and Prof. Dr. Maxim Y. Khlopov

MDPI

https://doi.org/10.3390/universe8110599

universe

MDPI

Article

Weak Deflection Angle by Kalb–Ramond Traversable Wormhole in Plasma and Dark Matter Mediums

Wajiha Javed [1], Hafsa Irshad [1], Reggie C. Pantig [2,3] and Ali Övgün [4,*]

[1] Department of Mathematics, Division of Science and Technology, University of Education, Lahore 54590, Pakistan
[2] Physics Department, De La Salle University, 2401 Taft Avenue, Manila 1004, Philippines
[3] Physics Department, Mapúa Institute of Technology, 658 Muralla St., Intramuros, Manila 1002, Philippines
[4] Physics Department, Eastern Mediterranean University, North Cyprus via Mersin 10, Famagusta 99628, Turkey
* Correspondence: ali.ovgun@emu.edu.tr

Abstract: This paper is devoted to computing the weak deflection angle for the Kalb–Ramond traversable wormhole solution in plasma and dark matter mediums by using the method of Gibbons and Werner. To acquire our results, we evaluate Gaussian optical curvature by utilizing the Gauss–Bonnet theorem in the weak field limits. We also investigate the graphical influence of the deflection angle $\tilde{\alpha}$ with respect to the impact parameter σ and the minimal radius r_0 in the plasma medium. Moreover, we derive the deflection angle by using a different method known as the Keeton and Petters method. We also examine that if we remove the effects of plasma and dark matter, the results become identical to that of the non-plasma case.

Keywords: general relativity; gravitational lensing; Gauss–Bonnet theorem; plasma medium; dark matter; Kalb–Ramond traversable wormhole; Keeton and Petters method

PACS: 95.30.Sf; 98.62.Sb; 97.60.Lf

Citation: Javed, W.; Irshad, H.; Pantig, R.C.; Övgün, A. Weak Deflection Angle by Kalb–Ramond Traversable Wormhole in Plasma and Dark Matter Mediums. *Universe* **2022**, *8*, 599. https://doi.org/10.3390/universe8110599

Academic Editors: Stefano Profumo and Jinmin Yang

Received: 8 September 2022
Accepted: 11 November 2022
Published: 13 November 2022

Publisher's Note: MDPI stays neutral with regard to jurisdictional claims in published maps and institutional affiliations.

1. Introduction

A visual illustration of a black hole (BH) shows that it dissipates energy through radiation, then compresses, and sooner or later dissolves [1]. Albert Einstein first estimated the presence of BHs by his theory of general relativity [2]. A BH is considered as an area of space having too strong a gravitational pull such that the fastest-moving objects and even light cannot escape it. Four types of BHs that exist are intermediate BHs, stellar BHs, miniature BHs, and supermassive BHs. Black holes are certainly very simple as they have two primary parts, the event horizon and the singularity. The event horizon is the boundary that indicates the limit of a BH. At the event horizon, the escape velocity becomes equal to the velocity of light. The singularity is a point in space where the existing mass has infinite density. According to GR, spacetime singularities lead to various issues, both scientifically and physically [3].

Just like BHs, wormholes (WHs) appear as effective solutions to the Einstein field equations. The simplest solution to the Einstein field equations is the Schwarzschild solution. The idea of a WH was first given by Flamm in 1916, soon after the invention of Schwarzschild's BH solution. In general, a WH is the link between two separate regions of space that are far away from each other via a tunnel [4]. In 1935, Einstein and Rosen [2] additionally investigated the theory of inter-universe connections. These spacetime connections were known to be "Einstein–Rosen Bridges". However, the idea of "WHs" was formulated by Wheeler in 1957 [5,6]. After that, he illustrated that WHs would be unsteady and non-traversable for even a photon.

Later on, the term traversable WH was developed by Morris and Thorne in 1988 [7]. They established flat traversable WHs with exotic matter that do not satisfy the null energy

conditions [8]. Exotic matter creates problems for making stable WHs. Morris, Thorne, and Yurtsever also showed that traversable WHs can be made stable and flat by applying the Casimir effect. Another type of traversable WH, a thin-shell WH, was introduced by Matt Visser in 1989 [9], in which a path through the WH may be made in such a way that the traversing path does not cross the region of exotic matter. Furthermore, the metric of the Ellis WH was considered firstly in [10], and the analysis of the Ellis WH returned in the standard work of Morris and Thorne, where they introduced traversable WHs. The deflection of light was initially suggested by Chetouani and Clement in the Ellis WH [11]. Nakajima and Asada also studied gravitational lensing by the Ellis WH [12].

It is a known fact that weak and strong gravitational lensing (GL) is a very productive area to find not only dark and heavy objects, but also BHs and WHs. To identify a WH, a possible way is the implementation of GL. The GL by WHs has been reviewed on a large scale in the literature of theoretical physics, as well as astrophysics [3,13–57].

Gravitational lensing was suggested by Soldner for the first time in the background of Newtonian theory. The basic theory of GL was formed by Liebes, Refsdal, and many other scientists [58–60]. When light released by distant galaxies passes through heavy objects in the universe, the gravitational attraction by those heavy objects can cause the light to deviate from its pathway. This process is known as GL. Gravitational lensing is a very applicable method to understand dark matter, galaxies, and the universe. Three types of GL listed in the literature are: (i) strong GL, (ii) weak GL, and (iii) micro-GL. Strong GL indicates the approximate magnification, location, and time delay of the images with the aid of BHs. Strong GL is also helpful to see various objects such as boson stars, fermion stars, and monopoles [61]. Weak GL is used to discover the mass of astronomical objects without demanding their changing nature. Weak lensing also differentiates dark energy from modified gravity and investigates how the universe is expanding rapidly. Gravitational lensing has been calculated for many spacetimes by applying various methods [51–84]. In the past few years, we have examined many research works that relate GL to the Gauss–Bonnet theorem (GBT).

Using the GBT, Gibbons and Werner [84] revealed that it is possible to compute the deflection angle in weak field limits using the Gauss–Bonnet theorem. After that, Werner expanded this technique to Kerr BHs [85] by using Nazim's method for the Randers–Finsler metric. Then, Ono et al. enlarged the study of weak GL in stationary axisymmetric spacetimes using the finite distance method [86–89]. The theory of GL comprises three physical processes named (i) geometric optics, (ii) the thin lens approximation, and (iii) the perturbation theory of GL [90–92].

For a distant observer from a source, the bending angle of light can be determined by using the GBT in the weak field limits [84]. By considering an oriented surface, let us describe a domain D_R surrounded by the beam of light with a circular boundary C_R having the Euler characteristic element $\mathcal{X}$ and metric g at the focus area where the light rays coincide with the source and the viewer. Therefore, when the GBT is applied within the optical metric, it provides us the bending angle of light stated as [84]:

$$\int\int_{\mathcal{D}_R} \mathcal{K} dS + \oint_{\partial \mathcal{D}_R} k dt + \sum_n \theta_n = 2\pi \mathcal{X}(\mathcal{D}_R),$$

where D_R is the region that comprises the source of the light waves, the observer, and the focal point of the lens, $\mathcal{K}$ shows the Gaussian optical curvature, dS is the surface element, k is known as geodesic curvature, and $\partial \mathcal{D}_R$ shows that this portion is surrounded by the outermost light rays. The asymptotic bending angle of light can be computed as [84]:

$$\tilde{\alpha} = -\int\int_{D_\infty} \mathcal{K} dS,$$

where $\tilde{\alpha}$ represents the bending angle and D_∞ indicates the infinite domain bounded by the rays of photons, apart from the lens. Moreover, by utilizing the GBT, the bending angle

for static and axisymmetric rotating Teo WHs was investigated by Jusufi and Övgün [93]. Recently, Övgün studied the deflection angle by Damour–Solodukhin WHs [94].

An approximate form of GL by the help of spherically symmetric lenses up to the post-post-Newtonian (PPN) was newly originated by Keeton and Petters [90,91]. Sereno and de Luca [92] expanded the PPN approximation to Kerr BHs. The Keeton and Petters method allows the calculations of those observable quantities that can be basically independent of coordinates and, therefore, physically applicable.

Dark matter comprises those particles that do not absorb, reflect, or emit light, so that they cannot be detected by observing electromagnetic radiation. Dark matter is a substance that cannot be directly visualized. Dark matter produces up to 27% of the overall mass–energy of the universe, and the remaining part consists of dark energy. Dark matter can only be noticed by its gravitational interaction. However, it has a weak non-gravitational interaction and is a non-relativistic nature [95]. Some of the dark matter exists as: weakly interacting massive particles (WIMPs), axions, sterile neutrinos, super WIMPs, etc. Dark matter particles are formed by non-baryonic particles. The neutrino is the only familiar non-baryonic particle, and it is taken as the first dark matter candidate. The refractive index used in dark matter maintains the propagation speed. According to the literature of the 20th Century, we have seen many times that matter mostly consists of protons and neutrons. However, the matter that we see is not a suitable form of matter. In this universe, there are some other types of matter whose masses are five-times greater than regular matter. Such unknown matter is called "dark matter". We have not been able to detect its existence in the laboratory until now. For the proper understanding of dark matter, we have to understand and then use various branches of astronomy and physics such as particle physics to describe the relation between dark matter and standard matter. Cosmology, general relativity, and astrophysics are applicable for the wide-ranging study of dark matter in the literature [96,97]. For the inspection of the bending angle through dark matter, we take the refractive index as [96,97]:

$$n(\omega) = 1 + \beta A_0 + A_2 \omega^2,$$

where ω is the frequency of a photon. It is noticed here that $\beta = \frac{\rho_0}{4m^2\omega^2}$ represents the mass density of the scattered dark matter particles, $A_0 = -2e^2\epsilon^2$ and $A_2 j \geq 0$. The higher-order terms such as $O(\omega^2)$ and onward are linked with the polarizability of the dark matter candidate. The term $O(\omega^2)$ stands for the neutral dark matter candidates, while $O(\omega^{-2})$ denotes the charged dark matter candidates.

The main goal of this paper is to examine the deflection of light for the Kalb–Ramond traversable WH solution by using various methods.

This paper is organized as follows. In Section 2, we analyze the Kalb–Ramond traversable WH solution in detail. In Section 3, we compute the deflection angle for the Kalb–Ramond traversable WH solution in the plasma medium. Section 4 is related to the graphical inspection of the deflection angle of the Kalb–Ramond traversable WH solution in the framework of the plasma medium. In Section 5, we investigate the bending angle of the Kalb–Ramond traversable WH solution by using the Keeton and Petters method. In Section 6, we enlarge our observations and derive the value of the deflection angle in the dark matter medium. In Section 7, we conclude all the results.

2. Kalb–Ramond Traversable Wormhole Solution

This section is devoted to describing some properties of a traversable WH solution. The metric is spherically symmetric and independent of time for the sake of simplification. A wormhole is like a tunnel connecting two regions of space, having no horizon because the presence of a horizon does not allow two-sided traveling. The time taken by the traveler to pass through the WH should be limited and fairly short. The gravitational force that the traveler inside the WH experiences should be slightly small.

Local Lorentz violation effects also result in modified gravitational dynamics. However, the Lorentz symmetry may be violated close to the Planck scale. When one or more

of the tensor fields gain nonzero vacuum expectation values (VEVs), Lorentz symmetry breaks spontaneously. The Kalb–Ramond (KR) field, an antisymmetric tensor field $B\mu\nu$ that appears in string theories, is another cause for spontaneous Lorentz symmetry breaking (LSB). A non-vanishing VEV breaks the gauge and the Lorentz symmetry by allowing a self-interaction potential. The tensor antisymmetric VEV can be split into two vectors, called pseudo-electric and pseudo-magnetic vectors, in the same way that the electromagnetic field strength can. A background KR field recently altered about a static and spherically symmetric WH. The parameter-dependent power-law correction to the Schwarzschild solution results from a non-minimal interaction between the KR VEV and the Ricci tensor. The effects of this LSB solution on the WH temperature and the shadows have also been investigated [98]. The static spherically symmetric spacetime of a Morris–Thorne traversable WH is expressed by the metric [7]:

$$ds^2 = -e^{2\phi(r)}dt^2 + \frac{dr^2}{1-\frac{\Omega(r)}{r}} + r^2 d\theta^2 + r^2 \sin^2\theta d\phi^2, \tag{1}$$

where the value of $\Omega(r)$ is defined as [98]:

$$\Omega(r) = r(\frac{r}{r_0})^{\frac{2}{1-2\lambda}}.$$

Here, λ is the Lorentz violating parameter $\lambda = |b|^2\xi_2$, b and ξ_2 are constants [98], $\phi(r)$ is the redshift function, and $\Omega(r)$ is the shape function of the WH. Both of these functions are adjustable. The redshift function is finite everywhere. The shape function $\Omega(r)$ calculates the shape of the WH or describes the WH physically. The radial variable r has a minimum value of r_0 and a maximum value of infinity, or $r_0 \leq r < \infty$. r_0 is a positive constant as it decreases from positive infinity to a least value and, after that, starts moving towards positive infinity.

After putting the value of the shape function, the spacetime metric becomes:

$$ds^2 = -dt^2 + \frac{dr^2}{1-(\frac{r}{r_0})^{\frac{2}{1-2\lambda}}} + r^2(d\theta^2 + \sin^2\theta d\phi^2). \tag{2}$$

Now, for the Kalb–Ramond traversable WH solution, we can write our metric in general form as:

$$ds^2 = -g_{tt}dt^2 + g_{rr}dr^2 + r^2 d\theta^2 + r^2 \sin^2\theta d\phi^2, \tag{3}$$

where,$g_{tt} = 1$ and $g_{rr} = \frac{1}{1-(\frac{r}{r_0})^{\frac{2}{1-2\lambda}}}$. For the calculation of the deflection angle by the Kalb–Ramond traversable WH solution, the optical path can be obtained by the null geodesic condition $ds^2 = 0$. Furthermore, we assume that the photon is moveable in the equatorial plane ($\theta = \frac{\pi}{2}$). In order to calculate the deflection angle, one can obtain the optical path metric in explicit form given as follows [98]:

$$dt^2 = \frac{dr^2}{1-(\frac{r}{r_0})^{\frac{2}{1-2\lambda}}} + r^2 d\phi^2. \tag{4}$$

The above metric will be used to calculate the deflection angle of light by the Kalb–Ramond traversable WH solution, which is described.

3. Deflection Angle in the Plasma Medium

In this section, we evaluate the impact of the plasma medium on weak GL for the Kalb–Ramond traversable WH solution (4). The value of the refractive index $n(r)$ for the given WH solution is defined as [99]:

$$n(r) = \sqrt{1 - \frac{\omega_e^2(r)}{\omega_\infty^2(r)}\Omega(r)}. \tag{5}$$

In the refractive index $n(r)$, ω_e indicates the plasma frequency of an electron, while ω_∞ denotes the frequency of a photon, which is noticed by the observer at infinity. Therefore, the optical metric can be written as:

$$dt^2 = g_{lm}^{opt} dx^l dx^m = n^2(r)\left[\frac{dr^2}{f(r)} + r^2 d\phi^2\right], \tag{6}$$

where $f(r)$ is defined as

$$f(r) = \frac{1}{1 - (\frac{r}{r_0})^{\frac{2}{1-2\lambda}}}. \tag{7}$$

Now, the relative Gaussian optical curvature can be determined by the expression present in [100,101]:

$$\mathcal{K} = \frac{R}{2}, \tag{8}$$

where R is the Ricci scalar. We calculate the Gaussian optical curvature for the Kalb–Ramond traversable WH solution as:

$$\mathcal{K} \simeq -\frac{r_0}{2r^3} + \frac{5}{4}\frac{r_0^2}{r^4}\frac{w_e^2}{w_\infty^2} - \frac{r_0}{r^3}\frac{w_e^2}{w_\infty^2} + \mathcal{O}(r_0^3). \tag{9}$$

The Gaussian curvature depends on minimal radius r_0 and radial parameter r. For the sake of simplicity, we consider the optical curvature up to order two, as well as to match our results given in the non-plasma medium case.

The infinitesimal surface element for the Kalb–Ramond traversable WH solution can be computed as:

$$dS = \sqrt{g} dr d\phi = \left(r - \frac{r w_e^2}{w_\infty^2}\right) dr d\phi + \mathcal{O}(r_0^3).$$

To find the deflection angle in the plasma medium, we utilize the GBT. As the beam of light approaches from infinity up to a large distance and remembering that we are present in weak field limitations, here, the beam of light becomes almost straight. Hence, we utilize the straight line approximation $r = \frac{\sigma}{\sin\phi}$, where σ expresses the impact parameter, and the GBT is stated as [84]:

$$\tilde{\alpha} = -\int_0^\pi \int_{\frac{\sigma}{\sin\phi}}^\infty \mathcal{K} dS. \tag{10}$$

The resulting expression can be expressed for $\lambda = \frac{3}{2}$. The Lorentz violating parameter must be restricted to the range $\lambda > 1/2$ to achieve an asymptotically flat spacetime. If we take $\lambda \simeq 0$, the geometry of the metric will not be asymptotically flat. For this value of λ, deflection angle $\tilde{\alpha}$ for the Kalb–Ramond traversable WH can be obtained as:

$$\tilde{\alpha} \simeq \frac{r_0}{\sigma} + \pi\left(\frac{r_0}{4\sigma}\right)^2 + \frac{w_e^2}{w_\infty^2}\frac{r_0}{\sigma} + \frac{r_0^2\pi}{8\sigma^2}\frac{w_e^2}{w_\infty^2} + \mathcal{O}(r_0^3). \tag{11}$$

The above result shows that the light rays are moving in the plasma medium. If we remove the plasma effects, this angle will convert into the non-plasma medium. The

deflection angle $\tilde{\alpha}$ depends on the minimal radius r_0 and the impact parameter σ, where the bending angle is directly proportional to r_0 and inversely proportional to σ.

4. Graphical Behavior of the Deflection Angle

This section is based on the explanation of the graphical analysis of the deflection angle for the Kalb–Ramond traversable WH solution in the plasma medium. For this purpose, we analyze the deflection angle with respect to the impact parameter σ and the minimal radius r_0.

4.1. $\tilde{\alpha}$ versus σ

Figure 1 shows the behavior of $\tilde{\alpha}$ with respect to the impact parameter σ for plasma impact $\frac{\omega_e}{\omega_\infty} = 10^{-1}$. For $r_0 \leq 3$, we observe that, in the first graph, as σ increases, $\tilde{\alpha}$ decreases exponentially and shows a convergent behavior, which converges to zero. On the other hand, we evaluated that, with the increase of r_0, the deflection angle also increases. Similarly, for $r_0 \geq 3$ in the second plot, the angle shows a decreasing behavior when the value of the impact parameter increases.

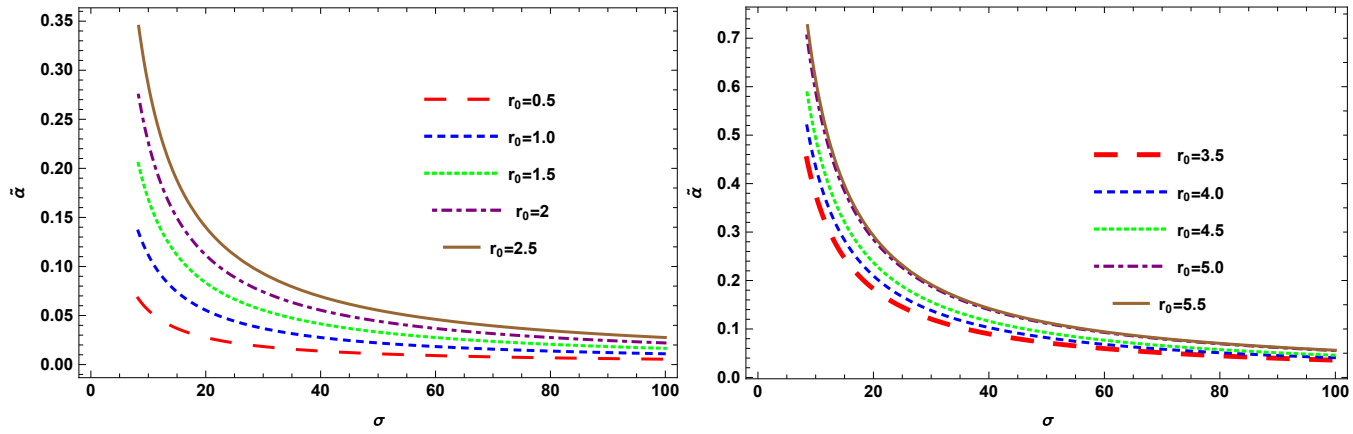

Figure 1. Figure 1 shows the behavior of $\tilde{\alpha}$ with respect to the impact parameter σ for plasma impact $\frac{\omega_e}{\omega_\infty} = 10^{-1}$.

Figure 2 shows that, for $r_0 \leq 3$, $r_0 > 3$ by assuming plasma impact $\frac{\omega_e}{\omega_\infty} = 10^{-2}$, one can analyze a similar behavior to that of $\frac{\omega_e}{\omega_\infty} = 10^{-1}$. We also investigated that, for small values of r_0, as σ increases, $\tilde{\alpha}$ exponentially decreases. Moreover, it is to be observed that, as the value of σ increases, $\tilde{\alpha}$ decreases. This shows that the deflection angle has an inverse relation with σ and a direct relation with r_0.

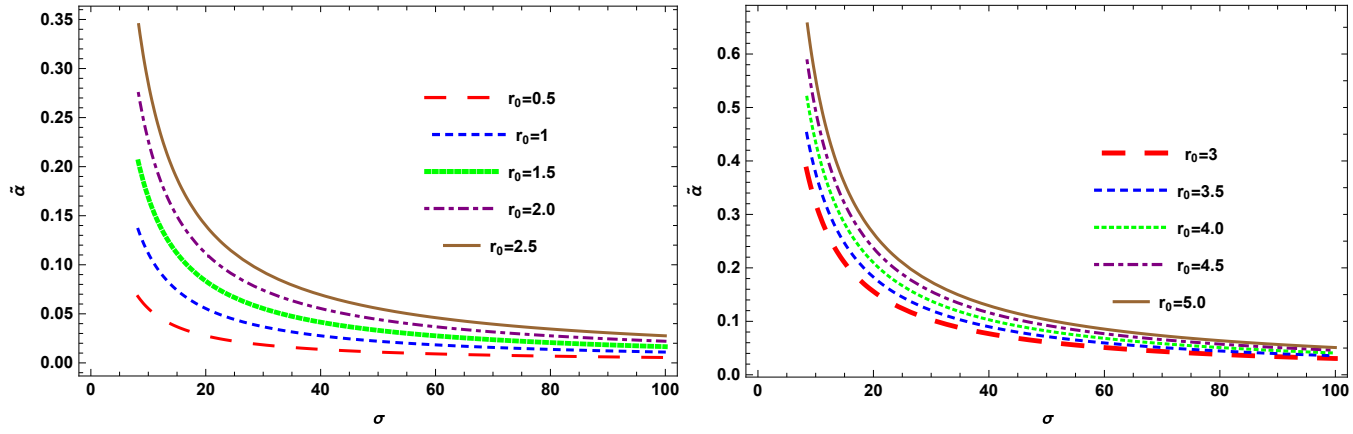

Figure 2. Figure 2 shows the behavior of $\tilde{\alpha}$ with respect to the impact parameter σ for plasma impact $\frac{\omega_e}{\omega_\infty} = 10^{-2}$.

4.2. $\tilde{\alpha}$ *versus* r_0

Figure 3 shows the behavior of the deflection angle $\tilde{\alpha}$ of the light with respect to r_0 for the impact parameter $0 < \sigma < 50$ and plasma impact $\frac{\omega_e}{\omega_\infty} = 10^{-1}$. We examine that for $0 < \sigma < 50$, the left graph indicates that as the linear behavior as r_0 increases, the bending angle $\tilde{\alpha}$ also increases, and as σ increases, the deflection angle decreases. For larger σ, the angle approaches zero. A similar case is given in the right plot for $\sigma > 50$: angle increases with increasing values of r_0, and vice versa.

Figure 4 shows that, for $\sigma > 50$ and $0 < \sigma \leq 50$ having plasma impact value $\frac{\omega_e}{\omega_\infty} = 10^{-2}$, we can analyze similar behavior as for the case $\frac{\omega_e}{\omega_\infty} = 10^{-1}$. We evaluated that as the values of r_0 increases, the deflection angle also increases, and as σ increases, the bending angle decreases, which shows the divergent behavior of the graphs. Furthermore, we investigated that bending angle $\tilde{\alpha}$ has a direct relation with impact parameter r_0 and an inverse relation with σ.

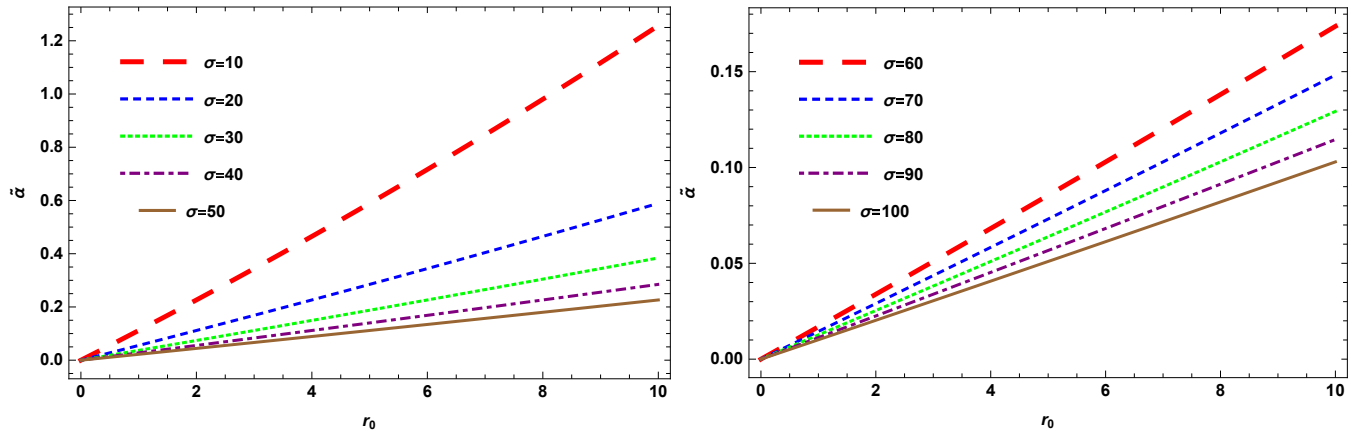

Figure 3. $\tilde{\alpha}$ versus r_0 for $\frac{\omega_e}{\omega_\infty} = 10^{-1}$.

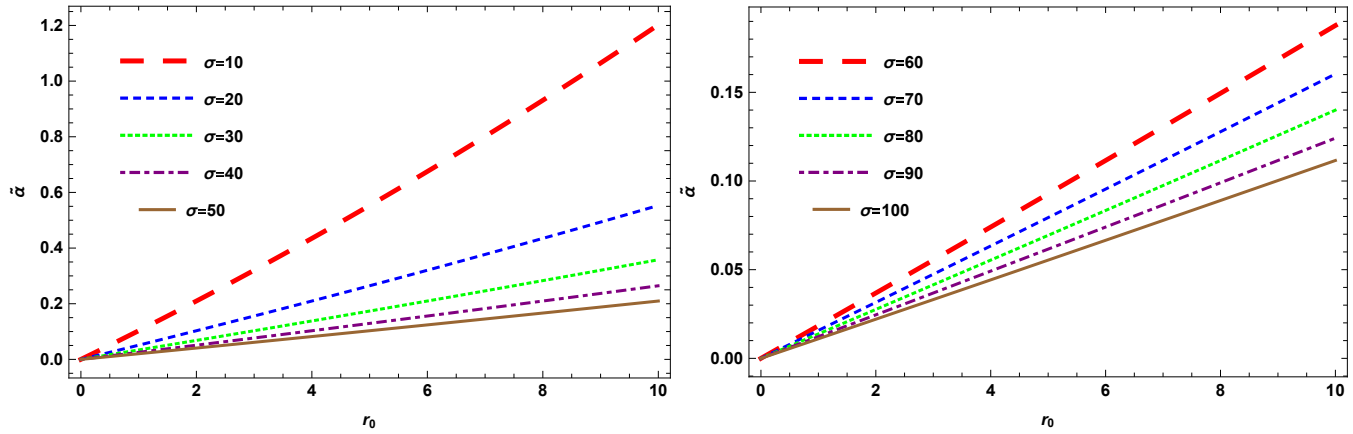

Figure 4. $\tilde{\alpha}$ versus r_0 for $\frac{\omega_e}{\omega_\infty} = 10^{-2}$.

5. Deflection Angle Using the Keeton and Petters Method

Keeton and Petters established a completely beneficial framework for computing corrections in a standard asymptotically flat metric theory of gravity [90,91]. The central focus is to illustrate a way to manage lensing in computing gravity theories using PPN corrections up to third-order.

The non-linear spherically symmetric and asymptotically Minkowski spacetime is defined by:

$$ds^2 = -A(r)dt^2 + B(r)dr^2 + C(r)d\Omega^2. \tag{12}$$

Due to the spherical symmetry, the geodesics of Equation (12) lie in the equatorial plane, while $d\Omega^2 = d\theta^2 + \sin^2\theta d\phi^2$ represents the standard unit metric. The above equation becomes:

$$ds^2 = -A(r)dt^2 + B(r)dr^2 + C(r)d\theta^2. \tag{13}$$

For $A(r) \to 1$, $B(r) \to 1$, and $C(r) \to r^2$, the spacetime metric is flat in the absence of the lens, and we suppose that A, B, and C are all +ve in the outside region of the lens from where the required light rays pass. The Kalb–Ramond traversable WH solution can be presented as:

$$ds^2 = -dt^2 + \frac{dr^2}{1 - (\frac{r}{r_0})^{\frac{2}{1-2\lambda}}} + r^2 d\theta^2, \tag{14}$$

where the metric functions are:

$$A(r) = 1, \tag{15}$$

and

$$B(r) = \frac{1}{1 - (\frac{r}{r_0})^{\frac{2}{1-2\lambda}}}. \tag{16}$$

To find the PPN coefficients, we compare the coefficients of the extended form of metric function with the coefficients of the standard form of the general metric in a PPN series to third-order. The general form of the PPN series for Eq.(5.1) given as [90]:

$$A(r) = 1 + 2a_1\left(\frac{\phi}{c^2}\right) + 2a_2\left(\frac{\phi}{c^2}\right)^2 + 2a_3\left(\frac{\phi}{c^2}\right)^3 ... \tag{17}$$

$$B(r) = 1 - 2b_1\left(\frac{\phi}{c^2}\right) + 4b_2\left(\frac{\phi}{c^2}\right)^2 - 8b_3\left(\frac{\phi}{c^2}\right)^3 ... \tag{18}$$

Here, ϕ denotes the three-dimensional Newtonian prospective. In our paper, we consider

$$\left(\frac{\phi}{c^2}\right) = \frac{r_0}{r}. \tag{19}$$

We obtain the values of the coefficients of PPN metric as

$$a_1 = 0, \;\; a_2 = 0, \;\; a_3 = 0, \;\; b_1 = \frac{1}{2}, \;\; b_2 = \frac{1}{4}, \;\; b_3 = \frac{1}{8}.$$

After finding the PPN coefficients, we then determine the coefficients in the extended form of the bending angle. The extended form of the light deflection angle can be written as follows

$$\alpha(b) = A_1\left(\frac{m}{b}\right) + A_2\left(\frac{m}{b}\right)^2 + A_3\left(\frac{m}{b}\right)^3 + O\left(\frac{m}{b}\right)^4. \tag{20}$$

We take $r_0 = m$ and $\sigma = b$. To compute the coefficients of the bending angle, we utilize the following equation:

$$\begin{aligned} A_1 &= 2(a_1 + b_1), \\ A_2 &= \left(2a_1^2 - a_2 + a_1 b_1 + b_2 - \frac{b_1^2}{4}\right)\pi, \\ A_3 &= \frac{2}{3}[35a_1^3 + 15a_1^2 b_1 - 3a_1\left(10a_2 + b_1^2 - 4b_2\right) \\ &+ 6a_3 + b_1^3 - 6a_2 b_1 - 4b_1 b_2 + 8b_3]. \end{aligned} \tag{21}$$

Using the Equation (21), we can determine the values of the coefficients presented as follows

$$A_1 = 1, \quad A_2 = \frac{3\pi}{16} \quad , A_3 = \frac{5}{12}.$$

After substituting the values of the coefficients in Equation (20), we obtain the resulting bending angle of the Kalb–Ramond traversable WH as:

$$\tilde{\alpha}(\sigma) = \left(\frac{r_0}{\sigma}\right) + \frac{3\pi}{16}\left(\frac{r_0}{\sigma}\right)^2 + \frac{5}{12}\left(\frac{r_0}{\sigma}\right)^3 + O\left(\frac{r_0}{\sigma}\right)^4. \tag{22}$$

This expression shows the deflection angle by using the Keeton and Petters method, which is dependent on r_0 and σ. The bending angle is directly proportional to r_0 and inversely proportional to σ.

6. Deflection Angle of a Photon in the Dark Matter Medium

Here, in this section, we examine how dark matter influences the weak deflection angle. For this purpose, we take the refractive index for the dark matter medium [42,96,97]:

$$n(\omega) = 1 + \beta A_0 + A_2\omega^2. \tag{23}$$

The two-dimensional optical geometry for the Kalb–Ramond traversable WH solution is:

$$dt^2 = n^2\left(\frac{dr^2}{1-(\frac{r}{r_0})^{\frac{2}{1-2\lambda}}} + r^2 d\phi^2\right), \tag{24}$$

with the condition:

$$\frac{dt}{d\phi}|_{C_R} = n\left(r^2\right)^{\frac{1}{2}}. \tag{25}$$

Applying this condition to a non-singular domain C_R outside of the light ray will yield the deflection angle. Hence, with the help of the GBT, we can calculate the weak deflection angle for the Kalb–Ramond traversable WH solution in the dark matter medium.

$$\lim_{R\to\infty}\int_0^{\pi+\alpha}\left[\mathcal{K}_g\frac{dt}{d\phi}\right]|_{C_R}d\phi = \pi - \lim_{R\to\infty}\int\int_{D_R}\mathcal{K}dS. \tag{26}$$

We compute the Gaussian optical curvature as follows:

$$\mathcal{K} = \frac{r_0}{2r_3(1+\beta A_0 + A_2\omega^2)}. \tag{27}$$

After this, we determine:

$$\lim_{R\to\infty}\mathcal{K}_g\frac{dt}{d\phi}|_{C_R} = 1. \tag{28}$$

Now, when we apply the limit $R \to \infty$, then we can evaluate the deflection angle for the Kalb–Ramond traversable WH solution by using the GBT as below:

$$\tilde{\alpha} = -\int_0^{\pi}\int_{\frac{\sigma}{\sin\phi}}^{\infty}\mathcal{K}dS. \tag{29}$$

We obtain the weak deflection angle of the Kalb–Ramond traversable WH solution in the dark matter medium after putting the value of $\mathcal{K}$ and dS:

$$\tilde{\alpha} \simeq \frac{r_0}{\sigma(1+\beta A_0 + A_2\omega^2)^6} + \frac{r_0^2\beta^6 A_0^{12}\pi}{16\sigma^2(1+\beta A_0 + A_2\omega^2)^6}| + \mathcal{O}(r_0^3). \tag{30}$$

This result shows that, when the effect of dark matter vanishes, the bending angle reduces to the deflection angle in the non-plasma medium. The effect of dark matter shows a larger deflection than in the general case. The deflection angle $\tilde{\alpha}$ depends on σ and r_0. We can see that dark matter gives a larger deflection angle than in the general case.

7. Conclusions

This paper was concerned with calculating the bending angle $\tilde{\alpha}$ for the Kalb–Ramond traversable WH solution in plasma and dark matter mediums. We evaluated the metric and explained its mathematical interpretation. For the calculation of the bending angle, we obtained the Gaussian optical curvature. After that, we applied the GBT and derived the value of the deflection angle for the Kalb–Ramond traversable WH solution in the plasma medium, Equation (11) for $\lambda = \frac{3}{2}$.

If we neglect or have the value of the plasma effect $\frac{\omega_e}{\omega_\infty}$ approach zero, then the effect of the plasma vanishes, and the resulting expression of the bending angle for the plasma medium reduces to the non-plasma case.

The graphical behavior of the deflection angle in the plasma medium was also calculated.

$\tilde{\alpha}$ with respect to impact parameter σ:

For $r_0 \leq 3$ and $r_0 > 3$ having the effect of the plasma $\frac{\omega_e}{\omega_\infty} = 10^{-1}$, the deflection angle $\tilde{\alpha}$ gradually approaches zero as σ increases, in both graphs. We have also observed that $\tilde{\alpha}$ exponentially decreases and indicates a convergent behavior for large values of σ. We examined that for $r_0 \leq 3$ and $r_0 > 3$ having the plasma effect $\frac{\omega_e}{\omega_\infty} = 10^{-2}$ as r_0 approaches infinity, $\tilde{\alpha} \to \infty$ at smaller σ. We also investigated that $\tilde{\alpha}$ has an inverse relation with σ and a direct relation with r_0.

$\tilde{\alpha}$ with respect to the minimal radius r_0:

We= analyzed that, for $0 < \sigma \leq 50$ and $\sigma > 50$, supposing $\frac{\omega_e}{\omega_\infty} = 10^{-1}$, the deflection angle $\tilde{\alpha}$ increases as the value of r_0 increases. The linear behavior of both graphs was examined. We also investigated that, as σ increases, the angle decreases, and vice versa. We reviewed that, for $0 < \sigma \leq 50$ and $\sigma > 50$ at $\frac{\omega_e}{\omega_\infty} = 10^{-2}$, deflection angle $\tilde{\alpha}$ exhibited similar behavior as that for $\frac{\omega_e}{\omega_\infty} = 10^{-1}$. We also examined that $\tilde{\alpha}$ increases for larger r_0 and $\tilde{\alpha}$ decreases as σ increases. We investigated a divergent behavior in both cases. We evaluated that $\tilde{\alpha}$ has a direct relationship with r_0 and an inverse relation with σ.

Furthermore, we also derived the deflection angle by using the Keeton and Petters, method which is the approximate form of GL, and used a spherically symmetric spacetime metric. For this purpose, we found the coefficients of the PPN metric by comparing the expanded metric function with the standard PPN metric. Later, we determined the coefficients of the bending angle and, again, by comparing them with the general form of Schwarzschild metric to obtain the final results given in Equation (22).

Lastly, we calculated the value of deflection angle $\tilde{\alpha}$ for the Kalb–Ramond traversable WH solution in the dark matter medium. Dark matter contains particles that cannot absorb, emit, or reflect light rays. For this purpose, we calculated Gaussian optical curvature Equation (27) and determined the deflection angle (30).

In the plasma, the Keeton and Petters method, and the dark matter medium case, the results reduced to the non-plasma case. The resulting equations depend on the minimal radius r_0 and impact parameter σ, showing that the deflection angle is directly proportional to r_0 and inversely to σ. The plots between the angle and minimal radius or impact parameter demonstrates that, when r_0 increases, the bending angle also move towards infinity. Furthermore, we observed the convergent and divergent behavior with respect to σ and r_0, respectively. When we removed the effect of plasma and dark matter, the resultant expression became similar to that of the Bumblebee traversable wormhole solution. In the case of the Keeton and Petters method, only the first term became similar to the general case.

Author Contributions: Conceptualization, W.J. and A.Ö.; methodology, R.C.P. and A.Ö.; software, H.I.; validation, W.J., R.C.P. and A.Ö.; formal analysis, H.I.; investigation, H.I.; resources, W.J. and A.Ö.; writing—original draft preparation, H.I.; writing—review and editing, W.J., H.I., R.C.P. and A.Ö.; visualization, H.I. and R.C.P.; supervision,W.J. and A.Ö. All authors have read and agreed to the published version of the manuscript.

Funding: This research received no external funding.

Data Availability Statement: Not applicable.

Acknowledgments: A.Ö. and R.C.P. would like to acknowledge networking support by the COST Action CA18108-Quantum gravity phenomenology in the multi-messenger approach (QG-MM).

Conflicts of Interest: The authors declare no conflict of interest.

References

1. Javed, W.; Abbas, G.; Ali, R. Charged vector particle tunneling from a pair of accelerating and rotating and 5D gauged supergravity black holes. *Eur. Phys. J. C* **2017**, *77*, 296. [CrossRef]
2. Einstein, A.; Rosen, N. The Particle Problem in the General Theory of Relativity. *Phys. Rev.* **1935**, *48*, 73–77. [CrossRef]
3. Javed, W.; Khadim, M.B.; Övgün, A.; Abbas, J. Weak gravitational lensing by stringy black holes. *Eur. Phys. J. Plus* **2020**, *135*, 314. [CrossRef]
4. Visser, M. *Lorentzian Wormholes: From Einstein to Hawking*; American Institute of Physics: New York, NY, USA, 1996.
5. Wheeler, J.A. Geons. *Phys. Rev.* **1955**, *97*, 511–536. [CrossRef]
6. Fuller, R.W.; Wheeler, J.A. Causality and Multiply Connected Space-Time. *Phys. Rev.* **1962**, *128*, 919–929. [CrossRef]
7. Morris, M.S.; Thorne, K.S. Wormholes in space-time and their use for interstellar travel: A tool for teaching general relativity. *Am. J. Phys.* **1988**, *56*, 395–412. [CrossRef]
8. Hochberg, D.; Visser, M. The Null energy condition in dynamic wormholes. *Phys. Rev. Lett.* **1998**, *81*, 746–749. [CrossRef]
9. Visser, M. Traversable wormholes: Some simple examples. *Phys. Rev. D* **1989**, *39*, 3182–3184. [CrossRef] [PubMed]
10. Ellis, H.G. Ether flow through a drainhole - a particle model in general relativity. *J. Math. Phys.* **1973**, *14*, 104–118. [CrossRef]
11. Chetouani, L.; Clement, L.G. Geometrical optics in the Ellis geometry. *Gen. Relat. Gravit.* **1984**, *16*, 111–119. [CrossRef]
12. Nakajima, K.; Asada, H. Deflection angle of light in an Ellis wormhole geometry. *Phys. Rev. D* **2012**, *85*, 107501. [CrossRef]
13. Kuhfittig, P.K.F. Gravitational lensing of wormholes in the galactic halo region. *Eur. Phys. J. C* **2014**, *74*, 2818. [CrossRef]
14. Tsukamoto, N.; Gong, Y. Extended source effect on microlensing light curves by an Ellis wormhole. *Phys. Rev. D* **2018**, *97*, 084051. [CrossRef]
15. Tsukamoto, N.; Harada, T. Light curves of light rays passing through a wormhole. *Phys. Rev. D* **2017**, *95*, 024030. [CrossRef]
16. Tsukamoto, N. Strong deflection limit analysis and gravitational lensing of an Ellis wormhole. *Phys. Rev. D* **2016**, *94*, 124001. [CrossRef]
17. Tsukamoto, N.; Gong, Y.; Retrolensing by a charged black hole. *Phys. Rev. D* **2017**, *95*, 064034. [CrossRef]
18. Tsukamoto, N. Deflection angle in the strong deflection limit in a general asymptotically flat, static, spherically symmetric spacetime. *Phys. Rev. D* **2017**, *95*, 064035. [CrossRef]
19. Övgün, A.; Sakallı, İ.; Saavedra, J. Shadow cast and Deflection angle of Kerr-Newman-Kasuya spacetime. *JCAP* **2018**, *10*, 41. [CrossRef]
20. Sakalli, I.; Övgün, A. Hawking Radiation and Deflection of Light from Rindler Modified Schwarzschild Black Hole. *EPL* **2017**, *118*, 60006. [CrossRef]
21. Övgün, A.; Jusufi, K.; Sakalli, I. Gravitational lensing under the effect of Weyl and bumblebee gravities: Applications of Gauss–Bonnet theorem. *Ann. Phys.* **2018**, *399*, 193–203. [CrossRef]
22. Övgün, A. Deflection Angle of Photons through Dark Matter by Black Holes and Wormholes Using Gauss–Bonnet Theorem. *Universe* **2019**, *5*, 115. [CrossRef]
23. Övgün, A.; Sakallı, İ.; Saavedra, J. Weak gravitational lensing by Kerr-MOG black hole and Gauss–Bonnet theorem. *Ann. Phys.* **2019**, *411*, 167978. [CrossRef]
24. Övgün, A.; Sakallı, İ. Testing generalized Einstein–Cartan–Kibble–Sciama gravity using weak deflection angle and shadow cast. *Class. Quant. Grav.* **2020**, *37*, 225003. [CrossRef]
25. Jusufi, K.; Werner, M.C.; Banerjee, A.; Övgün, A. Light Deflection by a Rotating Global Monopole Spacetime. *Phys. Rev. D* **2017**, *95*, 104012. [CrossRef]
26. Jusufi, K.; Övgün, A.; Saavedra, J.; Vásquez, Y.; González, P.A. Deflection of light by rotating regular black holes using the Gauss–Bonnet theorem. *Phys. Rev. D* **2018**, *97*, 124024. [CrossRef]
27. Javed, W.; Babar, R.; Övgün, A. The effect of the Brane-Dicke coupling parameter on weak gravitational lensing by wormholes and naked singularities. *Phys. Rev. D* **2019**, *99*, 084012. [CrossRef]
28. Övgün, A. Weak field deflection angle by regular black holes with cosmic strings using the Gauss–Bonnet theorem. *Phys. Rev. D* **2019**, *99*, 104075. [CrossRef]
29. Övgün, A.; Jusufi, K.; Sakallı, İ. Exact traversable wormhole solution in bumblebee gravity. *Phys. Rev. D* **2019**, *99*, 024042. [CrossRef]
30. Övgün, A.; Gyulchev, G.; Jusufi, K. Weak Gravitational lensing by phantom black holes and phantom wormholes using the Gauss–Bonnet theorem. *Ann. Phys.* **2019**, *406*, 152–172. [CrossRef]
31. Li, Z.; Övgün, A. Finite-distance gravitational deflection of massive particles by a Kerr-like black hole in the bumblebee gravity model. *Phys. Rev. D* **2020**, *101*, 024040. [CrossRef]
32. Javed, W.; Abbas, J.; Övgün, A. Deflection angle of photon from magnetized black hole and effect of nonlinear electrodynamics. *Eur. Phys. J. C* **2019**, *79*, 694. [CrossRef]

33. Javed, W.; Abbas, j.; Övgün, A. Effect of the Hair on Deflection Angle by Asymptotically Flat Black Holes in Einstein-Maxwell-Dilaton Theory. *Phys. Rev. D* **2019**, *100*, 044052. [CrossRef]
34. Jusufi, K.; Övgün, A.; Banerjee, A.; Sakallı, İ. Gravitational lensing by wormholes supported by electromagnetic, scalar, and quantum effects. *Eur. Phys. J. Plus* **2019**, *134*, 428. [CrossRef]
35. Javed, W.; Babar, R.; Övgün, A. Effect of the dilaton field and plasma medium on deflection angle by black holes in Einstein-Maxwell-dilaton-axion theory. *Phys. Rev. D* **2019**, *100*, 104032. [CrossRef]
36. Kumaran, Y.; Övgün, A. Weak Deflection Angle of Extended Uncertainty Principle Black Holes. *Chin. Phys. C* **2020**, *44*, 025101. [CrossRef]
37. Övgün, A.; Kumaran, Y.; Javed, W.; Abbas, J. Effect of Horndeski theory on weak deflection angle using the Gauss–Bonnet theorem. *Int. J. Geom. Meth. Mod. Phys.* **2022**, *19*, 2250192. [CrossRef]
38. Li, Z.; Zhang, G.; Övgün, A. Circular Orbit of a Particle and Weak Gravitational Lensing. *Phys. Rev. D* **2020**, *101*, 124058. [CrossRef]
39. Okyay, M.; Övgün, A. Nonlinear electrodynamics effects on the black hole shadow, deflection angle, quasinormal modes and greybody factors. *JCAP* **2022**, *1*, 9. [CrossRef]
40. Javed, W.; Abbas, J.; Övgün, A. Effect of the Quintessential Dark Energy on Weak Deflection Angle by Kerr-Newmann Black Hole. *Ann. Phys.* **2020**, *418*, 168183. [CrossRef]
41. Javed, W.; Hamza, A.; Övgün, A. Effect of nonlinear electrodynamics on the weak field deflection angle by a black hole. *Phys. Rev. D* **2020**, *101*, 103521. [CrossRef]
42. Övgün, A. Weak Deflection Angle of Black-bounce Traversable Wormholes Using Gauss–Bonnet Theorem in the Dark Matter Medium. *Turk. J. Phys.* **2020**, *44*, 465–471. [CrossRef]
43. Javed, W.; Khadim, M.B.; Övgün, A. Weak gravitational lensing by Bocharova–Bronnikov–Melnikov–Bekenstein black holes using Gauss–Bonnet theorem. *Eur. Phys. J. Plus* **2020**, *135*, 595. [CrossRef]
44. Çimdiker, İ.; Demir, D.; Övgün, A. Black hole shadow in symmergent gravity. *Phys. Dark Univ.* **2021**, *34*, 100900. [CrossRef]
45. Kumaran, Y.; Övgün, A. Deriving weak deflection angle by black holes or wormholes using Gauss–Bonnet theorem. *Turk. J. Phys.* **2021**, *45*, 247–267.
46. Javed, W.; Abbas, J.; Kumaran, Y.; Övgün, A. Weak deflection angle by asymptotically flat black holes in Horndeski theory using Gauss–Bonnet theorem. *Int. J. Geom. Meth. Mod. Phys.* **2021**, *18*, 2150003. [CrossRef]
47. Pantig, R.C.; Övgün, A. Dark matter effect on the weak deflection angle by black holes at the center of Milky Way and M87 galaxies. *Eur. Phys. J. C* **2022**, *82*, 391. [CrossRef]
48. Pantig, R.C.; Övgün, A. Dehnen halo effect on a black hole in an ultra-faint dwarf galaxy. *JCAP* **2022**, *8*, 56. [CrossRef]
49. Pantig, R.C.; Rodulfo, E.T. Weak deflection angle of a dirty black hole. *Chin. J. Phys.* **2020**, *66*, 691–702. [CrossRef]
50. Pantig, R.C.; Yu, P.K.; Rodulfo, E.T.; Övgün, A. Shadow and weak deflection angle of extended uncertainty principle black hole surrounded with dark matter. *Ann. Phys.* **2022**, *436*, 168722. [CrossRef]
51. Sharif, M.; Iftikhar, S. Strong gravitational lensing in non-commutative wormholes. *Astrophys. Space Sci.* **2015**, *357*, 85. [CrossRef]
52. Shaikh, R.; Kar, S. Gravitational lensing by scalar-tensor wormholes and the energy conditions. *Phys. Rev. D* **2017**, *96*, 044037. [CrossRef]
53. Sajadi, S.N.; Riazi, N. Gravitational lensing by multi-polytropic wormholes. *Can. J. Phys.* **2020**, *98*, 1046–1054. [CrossRef]
54. Asada, H. Gravitational lensing by exotic objects. *Mod. Phys. Lett. A* **2017**, *32*, 1730031. [CrossRef]
55. Yoo, C.M.; Harada, T.; Tsukamoto, N. Wave Effect in Gravitational Lensing by the Ellis Wormhole. *Phys. Rev. D* **2013**, *87*, 084045. [CrossRef]
56. Tsukamoto, N.; Harada, T.; Yajima, K. Can we distinguish between black holes and wormholes by their Einstein ring systems? *Phys. Rev. D* **2012**, *86*, 104062. [CrossRef]
57. Bhattacharya, A.; Potapov, A.A. Bending of light in Ellis wormhole geometry. *Mod. Phys. Lett. A* **2010**, *25*, 2399–2409. [CrossRef]
58. Liebes, J. Gravitational Lenses. *Phys. Rev.* **1964**, *133*, 835. [CrossRef]
59. Refsdal, S. The gravitational lens effect. *Mon. Not. Roy. Astron. Soc.* **1964**, *128*, 295. [CrossRef]
60. Pantig, R.C.; Mastrototaro, L.; Lambiase, G.; Övgün, A. Shadow, lensing and neutrino propagation by dyonic ModMax black holes. *arXiv* **2022**, arXiv:2208.06664.
61. Barriola, M.; Vilenkin, A. Gravitational Field of a Global Monopole. *Phys. Rev. Lett.* **1989**, *63*, 341. [CrossRef]
62. Keeton, C.R.; Kochanek, C.S.; Falco, E.E. The Optical properties of gravitational lens galaxies as a probe of galaxy structure and evolution. *Astrophys. J.* **1998**, *509*, 561–578. [CrossRef]
63. Eiroa, E.F.; Romero, G.E.; Torres, D.F. Reissner-Nordstrom black hole lensing. *Phys. Rev. D* **2002**, *66*, 024010. [CrossRef]
64. Uniyal, A.; Pantig, R.C.; Övgün, A. Probing a nonlinear electrodynamics black hole with thin accretion disk, shadow and deflection angle with M87* and Sgr A* from EHT. *arXiv* **2022**, arXiv:2205.11072.
65. Pantig, R.C.; Övgün, A. Testing dynamical torsion effects on the charged black hole's shadow, deflection angle and greybody with M87* and Sgr A* from EHT. *arXiv* **2022**, arXiv:2206.02161.
66. Rayimbaev, J.; Pantig, R.C.; Övgün, A.; Abdujabbarov, A.; Demir, D. Quasiperiodic oscillations, weak field lensing and shadow cast around black holes in Symmergent gravity. *arXiv* **2022**, arXiv:2206.06599.
67. Mustafa, G.; Atamurotov, F.; Hussain, I.; Shaymatov, S.; Övgün, A. Shadows and gravitational weak lensing by the Schwarzschild black hole in the string cloud background with quintessential field. *arXiv* **2022**, arXiv:2207.07608.

68. Kuang, X.M.; Övgün, A. Strong gravitational lensing and shadow constraint from M87* of slowly rotating Kerr-like black hole. *Ann. Phys.***2022**, *447*, 169147. [CrossRef]
69. Javed, W.; Riaz, S.; Övgün, A. Weak Deflection Angle and Greybody Bound of Magnetized Regular Black Hole. *Universe* **2022**, *8*, 262. [CrossRef]
70. Javed, W.; Hussain, I.; Övgün, A. Weak deflection angle of Kazakov–Solodukhin black hole in plasma medium using Gauss–Bonnet theorem and its greybody bonding. *Eur. Phys. J. Plus* **2022**, *137*, 148. [CrossRef]
71. Javed, W.; Khadim, M.B.; Övgün, A. Weak gravitational lensing by Einstein-nonlinear-Maxwell–Yukawa black hole. *Int. J. Geom. Meth. Mod. Phys.* **2020**, *17*, 2050182. [CrossRef]
72. Moumni, H.E.; Masmar, K.; Övgün, A. Weak deflection angle of light in two classes of black holes in nonlinear electrodynamics via Gauss–Bonnet theorem. *Int. J. Geom. Meth. Mod. Phys.* **2022**, *19*, 2250094. [CrossRef]
73. Belhaj, A.; Belmahi, H.; Benali, M.; El, H.M. Light Deflection by Rotating Regular Black Holes with a Cosmological Constant. *arXiv* **2022**, arXiv:2204.10150.
74. Belhaj, A.; Belmahi, H.; Benali, M.; Moumni, H.E. Light deflection angle by superentropic black holes. *Int. J. Mod. Phys. D* **2022**, *31*, 2250054. [CrossRef]
75. Belhaj, A.; Benali, M.; Balali, A.E.; Moumni, H.E.; Ennadifi, S.E. Deflection angle and shadow behaviors of quintessential black holes in arbitrary dimensions. *Class. Quant. Grav.* **2020**, *37*, 215004. [CrossRef]
76. Javed, W.; Aqib, M.; Övgün, A. Effect of the magnetic charge on weak deflection angle and greybody bound of the black hole in Einstein-Gauss–Bonnet gravity. *Phys. Lett. B* **2022**, *829*, 137114. [CrossRef]
77. Javed, W.; Hamza, A.; Övgün, A. Weak Deflection Angle and Shadow by Tidal Charged Black Hole. *Universe* **2021**, *7*, 385. [CrossRef]
78. Bozza, V. Gravitational lensing in the strong field limit. *Phys. Rev. D* **2002**, *66*, 103001. [CrossRef]
79. Virbhadra, K.S.; Ellis, G.F.R. Schwarzschild black hole lensing. *Phys. Rev. D* **2000**, *62*, 084003. [CrossRef]
80. Virbhadra, K.S.; Ellis, G.F.R. Gravitational lensing by naked singularities. *Phys. Rev. D* **2002**, *65*, 103004. [CrossRef]
81. Virbhadra, K.S.; Narasimha, D.; Chitre, S.M. Role of the scalar field in gravitational lensing. *Astron. Astrophys.* **1998**, *337*, 1–8.
82. Virbhadra, K.S.; Keeton, C.R. Time delay and magnification centroid due to gravitational lensing by black holes and naked singularities. *Phys. Rev. D* **2008**, *77*, 124014. [CrossRef]
83. Virbhadra, K.S. Relativistic images of Schwarzschild black hole lensing. *Phys. Rev. D* **2009**, *79*, 083004. [CrossRef]
84. Gibbons, G.W.; Werner, M.C. Applications of the Gauss–Bonnet theorem to gravitational lensing. *Class. Quant. Grav.* **2008**, *25*, 235009. [CrossRef]
85. Werner, M.C. Gravitational lensing in the Kerr-Randers optical geometry. *Gen. Relativ. Gravit.* **2012**, *44*, 3047–3057. [CrossRef]
86. Ono, T.; Ishihara, A.; Asada, H. Gravitomagnetic bending angle of light with finite-distance corrections in stationary axisymmetric spacetimes. *Phys. Rev. D* **2017**, *96*, 104037. [CrossRef]
87. Ono, T.; Ishihara, A.; Asada, H. Deflection angle of light for an observer and source at finite distance from a rotating wormhole. *Phys. Rev. D* **2018**, *98*, 044047. [CrossRef]
88. Ono, T.; Ishihara, A.; Asada, H. Deflection angle of light for an observer and source at finite distance from a rotating global monopole. *Phys. Rev. D* **2019**, *99*, 124030. [CrossRef]
89. Takizawa, K.; Ono, T.; Asada, H. Gravitational deflection angle of light: Definition by an observer and its application to an asymptotically nonflat spacetime. *Phys. Rev. D* **2020**, *101*, 104032. [CrossRef]
90. Keeton, C.R.; Petters, A.O. Formalism for testing theories of gravity using lensing by compact objects. I. Static, spherically symmetric case. *Phys. Rev. D* **2005**, *72*, 104006. [CrossRef]
91. Keeton, C.R.; Petters, A.O. Formalism for testing theories of gravity using lensing by compact objects. II. Probing post-post-Newtonian metrics. *Phys. Rev. D* **2006**, *73*, 044024. [CrossRef]
92. Sereno, M.; Luca, F.D. Analytical Kerr black hole lensing in the weak deflection limit. *Phys. Rev. D* **2006**, *74*, 123009. [CrossRef]
93. Jusufi, K.; Övgün, A. Gravitational Lensing by Rotating Wormholes. *Phys. Rev. D* **2018**, *97*, 024042. [CrossRef]
94. Övgün, A. Light deflection by Damour-Solodukhin wormholes and Gauss–Bonnet theorem. *Phys. Rev. D* **2018**, *98*, 044033. [CrossRef]
95. Feng, J.L. Dark Matter Candidates from Particle Physics and Methods of Detection. *Ann. Rev. Astron. Astrophys.* **2010**, *48*, 495–545. [CrossRef]
96. Latimer, D.C. Dispersive Light Propagation at Cosmological Distances: Matter Effects. *Phys. Rev. D* **2013**, *88*, 063517. [CrossRef]
97. Latimer, D.C. Anapole dark matter annihilation into photons. *Phys. Rev. D* **2017**, *95*, 095023. [CrossRef]
98. Lessa, L.A.; Oliveira, R.; Silva, J.E.G.; Almeida, C.A.S. Traversable wormhole solution with a background Kalb–Ramond field. *Ann. Phys.* **2021**, *433*, 168604. [CrossRef]
99. Crisnejo, G.; Gallo, E. Weak lensing in a plasma medium and gravitational deflection of massive particles using the Gauss–Bonnet theorem. A unified treatment. *Phys. Rev. D* **2018**, *97*, 124016. [CrossRef]
100. Jusufi, K.; Övgün, A.; Banerjee, A. Light deflection by charged wormholes in Einstein-Maxwell-dilaton theory. *Phys. Rev. D* **2017**, *96*, 084036. [CrossRef]
101. Arakida, H. Light deflection and Gauss–Bonnet theorem: Definition of total deflection angle and its applications. *Gen. Relativ. Gravit.* **2018**, *50*, 48. [CrossRef]